Journal of Energy Storage 20 (2018) 418–426

Contents lists available at ScienceDirect

Journal of Energy Storage

journal homepage: www.elsevier.com/locate/est

Synthesis and characterization of activated carbon from the biomass of *Saccharum bengalense* for electrochemical supercapacitors

Sangeeta Rawal[a,1], Bhawana Joshi[a,*], Yogesh Kumar[b,1]

[a] Department of Applied Physics, Gautam Buddha University, Greater Noida, Uttar Pradesh, 201308, India
[b] Department of Physics, ARSD College, University of Delhi, New Delhi, 110021, India

ARTICLE INFO

Keywords:
Saccharum bengalense
Bio-resource derived carbon
Electrical double layer capacitors
Activated carbon
Aqueous electrolyte (Li_2SO_4)
$ZnCl_2$ activating agent

ABSTRACT

Low cost and very simple activation method ($ZnCl_2$ as activating agent) is used for the synthesis of activated carbon derived from the biomass of *Saccharum bengalense (S. bengalense)* leaves. The *S. bengalense* derived activated carbon (SbAC) as the electrode material in Electric Double Layer Capacitors (EDLCs) is reported for the first time. The structural, surface morphological study and vibrational response of the SbAC are characterized by using X-ray diffraction (XRD), Field Emission Scanning Electron Microscopy (FE-SEM), Fourier Transform Infrared Spectroscopy (FTIR), Raman spectroscopy, and Brunauer-Emmett-Teller (BET) surface area. Electrochemical studies indicate that the SbAC delivers the maximum specific capacitance of 102.6 F g^{-1}at scan rate of 2 mV/s in aqueous electrolyte (1 M Li_2SO_4) for 1.6 V operating voltage. This high value of specific capacitance is credited to its high specific surface area (2090 $m^2 g^{-1}$) and pore volume of 0.281 $cm^3 g^{-1}$. The SbAC exhibits good rate capability with an excellent charging/discharging cycle stability in aqueous electrolyte (1 M Li_2SO_4) during 120,000 cycles. The results indicate that SbAC shows good electrochemical properties to be used for energy storage applications in future.

1. Introduction

To meet the sustainable energy requirement for world's increasing population these days the use of harmful chemicals and non-renewable resources is continuously increasing. The deteriorating environmental issues caused due to the use of harmful chemicals such as lithium, nickel, cadmium and non-renewable resources in making energy devices has forced the mankind to think beyond the limited and non-renewable fossil fuels. Henceforth, renewable and non-fossil-based energy resources have been used to build a sustainable future for our coming generations. These renewable sources can be wind, solar energy and biomass etc. From the last two decades supercapacitors (SCs) or electrochemical capacitors are being considered as a good source of the next-generation energy storage devices along with other batteries and fuel cells. EDLCs, which store the charge electrostatically at the electrode surface of very porous and high specific surface area electrode material, are being considered for energy storage devices in various applications [1].

These days another class of SCs, known as hybrid capacitors also, have been adopted which are a combination of EDLCs and the pseudocapacitors (transition metal oxides or conducting polymers) to improve the specific capacitance and energy density. These hybrid capacitors can be made with various configuration of metal oxide, conducting polymers and different forms of carbon. One such configuration is made by mixing the metal oxides or conducting polymer with different carbon material to make hybrid electrode material. Such as activated carbon is mixed with sodium phosphate or maricite ($NaMn_{1/3}Ni_{1/3}Co_{1/3}PO_4$) to make a hybrid capacitor for the very first time [2]. $NaMn_{1/3}Ni_{1/3}Co_{1/3}PO_4$/activated carbon based hybrid capacitor was found to have energy density of 15 W h kg^{-1} along with good power density of 400 W kg^{-1} in aqueous electrolyte (NaOH). Another class of hybrid consists of both the electrodes made up of different materials. M Minakshi *et al* prepared a hybrid capacitor with $MMoO_4$ with biopolymer additive as the positive electrode (cathode) and AC as the negative electrode (anode), studied its electrochemical properties in aqueous electrolyte (2 M NaOH) and observed good capacitance values up to 124 F g^{-1} [3]. R. Ramkumar *et al* studied the electrochemical properties of the polyaniline coated graphite and PANI/$NiMoO_4$ composite and found that the PANI/$NiMoO_4$ composite showed higher capacitance value of 685 m F cm^{-2} as compared to the low capacitance value of PANI coated carbon (247 m F cm^{-2}). In the hybrid capacitor of PANI/$NiMoO_4$ composite higher capacitance is observed due the redox

* Corresponding author.
E-mail addresses: bhawana@gbu.ac.in (B. Joshi), ykumar@arsd.physics.du.ac.in (Y. Kumar).
[1] These authors contributed equally.

https://doi.org/10.1016/j.est.2018.10.009
Received 9 July 2018; Received in revised form 1 October 2018; Accepted 7 October 2018
Available online 24 October 2018
2352-152X/

phenomena of the Ni ions [4]. Doping of heteroatom (such as N, P, S etc) in activated carbon or carbon nanotubes coated with conductive polymer has also shown noticeable increase in the specific surface area, specific capacitance and energy density. K. Shi *et al* used the polypyrrole coated multiwalled carbon nanotubes for the coating of N doped activated carbon (N-AC-MWCNT). It was observed that the N doped activated carbon coated with multi walled carbon nanotubes shows high increase in specific area (1889.12 m^2 g^{-1}) as compared to multiwalled carbon nanotubes (325.48 m^2 g^{-1}) and N doped carbon (489.39 m^2 g^{-1}) due to which they found applications in capacitive dye removal technologies [5]. The use of N-AC-MWCNT shows good electrochemical properties in asymmetric configuration. In asymmetric configuration N-AC-MWCNT is coated with MnO_2 for positive electrode and negative electrode is made up of N-AC-MWCNT with a high mass loading of 20 mg cm^{-2} and it showed high specific capacitance 311.7 F g^{-1} [6]. Doping of N in activated carbon nanofibers (N-AC-NF) enhances the specific surface area and makes it suitable for capacitive dye removal application [7].

EDLCs can be utilized in a large number of applications such as in aerospace, defence, consumer electronics, medical services and un-interruptible power sources. In hybrid electric vehicles these supercapacitors are being used along with batteries [8]. In many energy storing devices various kinds of non-regenerative and harmful chemicals are used as the resource material. So, to avoid the use of these non-regenerative fossil fuels and harmful chemical and to meet the continuously increasing requirement of high energy and power densities, new resources with good electrochemical properties need to be discovered [9]. One such resource is biomass which can be considered as a good source for activated carbon because it is cheaper, renewable, easily available, low cost, environment friendly and being a lignocellulosic material gives good carbon content. From the literature reports it can be concluded that activated carbon is a good candidate for the supercapacitor electrode material. It can have specific surface area (SSA) as high as 3000 m^2 gm^{-1} [11] and high value of surface area is favourable for the adsorption of more ions on the electrode surface to form a double layer in EDLCs. The presence of hetero-atoms such as oxygen, nitrogen etc. in carbon framework gives surplus advantage of reversible faradaic reactions [9–11].

Various methods have been used for the synthesis of activated carbon inclusive of carbonisation, hydrothermal, pyrolysis and activation method. Out of all these activated carbon synthesis methods, activation methods are very simple, low cost and less time consuming. Activation method involves two steps carbonisation followed by activation. Activation can be chemical or physical depending on whether an activating agent is used or not. In the activation method the surface area, pore sizes and pore structures of the activated carbon can be tailored by controlling the synthesis parameters such as temperature, time, pressure and activating agent.

The manufacturing of the activated carbon is mainly obtained from natural bio-resource, different bio-waste, mines and synthetic precursors. The use of activated carbons to healthcare, cosmetics and living organisms requires a safe, biocompatible and cheaper resource. From the above-mentioned resources, the activated carbons from bio-waste, mines and synthetic precursors contain a significant level of heavy metal and toxic contamination, even after proper cleaning and washing. The supply of the activated carbon to the industry is a greater challenge in recent times. Innovative uses of the activated carbons have increased the demand enormously around the globe. Freedonia group reports that the demand for activated carbon is estimated to rise approximately 8.1% per year to 2.1 million metric tons in 2018. To meet this increasing demand of active carbon these days various biomass resources such as waste coffee beans [12], cassava peel waste [13], various nutshells [14], rice husk [15], sunflower seed shell [16], coffee endocarp [17], rubber wood sawdust [18], oil bamboo wastes [19], peanut shell [20] and many other biomass precursors have been considered as for preparing porous carbon material.

In this paper such new resource *Saccharum bengalense* is used for the synthesis of activated carbon. *S. bengalense* is a safe, biocompatible, non-toxic and ecologically available resource for activated carbon synthesis. So, *S. Bengalense* plant has been very useful from decades for many rural applications but it has not been used till now for the synthesis of porous activated carbon to be used for supercapacitor applications. However, other members of the saccharum family have been explored for supercapacitor applications. In this paper, we report the preparation of porous carbon materials using *S. bengalense* by $ZnCl_2$ chemical activation method and the study of its electrochemical properties in aqueous electrolyte (1 M Li_2SO_4) very first time. The resulting product has a good porous structure along with high specific surface area which makes it suitable candidate for low-cost electrode material for EDLC applications. The botanical information about the *Saccharum bengalense* plant can be obtained in the supporting information related to this paper.

2. Experimental

2.1. Synthesis of S. bengalense derived activated carbon (SbAC)

Chemical activation method is used for the synthesis of activated carbon from *S. Bengalense* by following the Hu *et al.* method [21]. The exact procedure and steps for the preparation and its activation are shown in Fig. 1. The fresh *S. bengalense* leaves were washed thoroughly and dried. These leaves were then crushed to a fine powder form and mixed with an activating agent $ZnCl_2$ in the presence of de-ionised water to form a slurry. $ZnCl_2$ acts as activating agent and helps in the making of good porous structure. The slurry was then heated to 800 °C in an inert atmosphere for 30 min to get at least 20% yield. Here this inert atmosphere is provided by the constant flow of N_2 gas at a rate of 5 °C/min with 100 cm^3/min flow rate. The resultant material was washed thoroughly by dilute HCl (for the removal of zinc compounds) and with hot de-ionized water (to remove chloride ions). Finally, the resultant material was dried for 12 h in a vacuum oven at 110 °C to obtain the *S. bengalense* derived activated carbon (SbAC). The ratio of the biomass to the activating agent ($ZnCl_2$), final temperature, duration of heating and the rate of the inert gas are the controlling parameters and play a crucial role in the formation of high porosity and specific surface area of the final activated carbon material.

2.2. Preparation of electrode and fabrication of EDLC cell

Polyvinylidene fluoride-co-hexafluoropropylene (PVdF-HFP) is used to bind synthesized activated porous carbon as it was very porous to be used as an electrode material in the cell. PVdF-HFP, conductive additive acetylene black and SbAC are mixed in the 85:10:5 ratio respectively. A slurry is prepared from the mixture by adding appropriate amount of acetone. Graphite sheets were used to make electrodes and the prepared slurry was coated on it by spin coating method. 1 mg cm^{-2} of the synthesized activated carbon is used on each electrode for the supercapacitor cell. The SbAC electrodes are vacuum dried before using them for making EDLC cells. An aqueous electrolyte 1 M Li_2SO_4 is used as the electrolyte between the two electrodes separated by a separator.

2.3. Characterization

The synthesized SbAC was characterized using Bruker AXS, D8 advance X-ray diffractometer to obtain its X-Ray diffraction pattern. The diffractometer was operated at 20 kV and 40 mA using Cu Kα radiation having a wavelength of 1.5418 Å. The sample was scanned through a 2θ range of 10–80°. Thermo Gravimetric Analysis (TGA), Differential Thermal Analysis (DTA) and Differential Thermo Gravimetry (DTG) were carried out using a EXSTAR TG/DTA 6300, in inert atmosphere (pure nitrogen) with a flow rate of 200 ml/min, at a constant heating

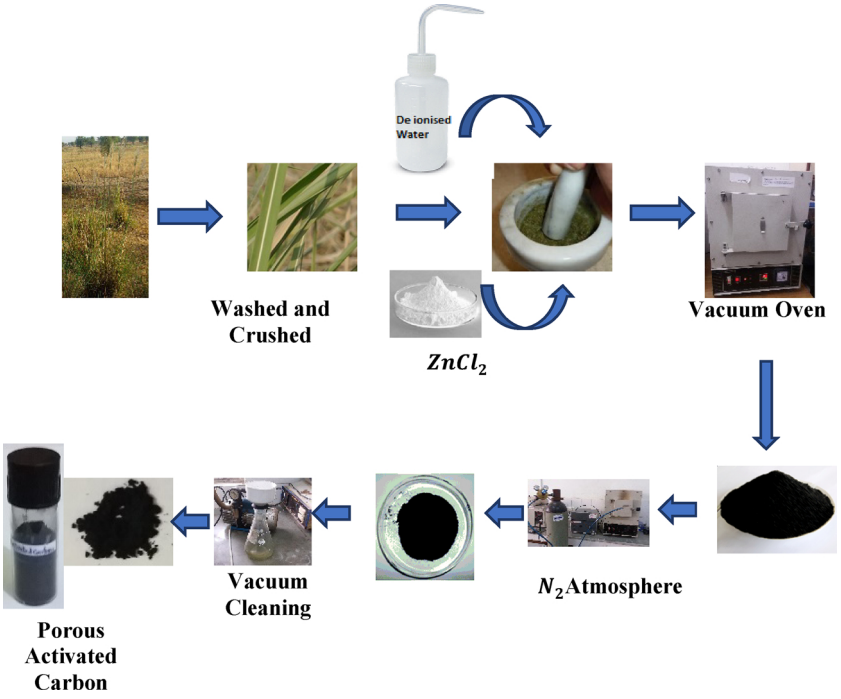

Fig. 1. Flow diagram for S. bengalense derived activated carbon (SbAC).

rate of 10 °C/min by varying the temperature from room temperature (24 °C) to 700 °C. The initial mass for the TGA was 10.48 mg and the spectra were collected in transmittance mode. Renishaw Invia Raman Microscope was used to carry out the Raman measurements using the Ar-ion laser (50 mW) at a resolution of 3 cm^{-1}. Fourier Transform Infrared (FTIR) spectra was obtained by a Nicolet NEXUS Aligent, 1100 using KBr powder pressed pellets in the range 500–4000 cm^{-1} at a resolution of 1 cm^{-1}. Surface morphology was seen by Carl Zeiss model Ultra Plus Field Emission Scanning Electron Microscope (FE-SEM) fitted with an Energy Dispersive X-ray (EDX) spectroscope. The Brunauer-Emmett-Teller (BET) method was used to determine the specific surface area, pore size and pore volume of the prepared material by physisorption of nitrogen on a Micromet-rics ASAP 2010 analyzer. The relative pressure (P/P_0) is varied from 0 to 1.0 to obtain the adsorption data.

2.4. Electrochemical measurements

Electrochemical Impedance Spectroscopy (EIS), Cyclic Voltagram (CV), Galvanostatic charge–discharge and other electrochemical techniques were used for the electrochemical measurements of the prepared electrodes from SbAC. Electrochemical analyzer with model number 608C; CH Instrument was used for the recording the CV measurements. A charge–discharge unit (model BT-2000; Arbin Instruments, USA) was used for recording the galvanostatic charge–discharge characteristics of the cells. Impedance/Gain-Phase Analyzer (Solartron 1260) was used for measuring the EIS characteristics of the electrodes for low to high frequency range which in this case is 10 mHz to 100 kHz.

3. Results and discussion

3.1. Structural and morphological properties

The structure analysis of SbAC was carried out using powder XRD analysis and Raman spectroscopy. Fig. 2(a) shows the diffraction pattern of the as-synthesized SbAC material showing two strong and broad diffraction peaks at 24.7° and 43.6° which corresponds to the (002) planes and (001) planes of the graphitic carbon (JCPDS No. 75-1621) [22]. It is observed that SbAC shows the graphitic like microcrystalline that contain small disordered structure. High intensity in the low angle region may be due to large ratio of micropores in SbAC which was further confirmed from the N_2 adsorption-desorption measurements as shown in Fig. 5.

Thermal behaviour of the SbAC was studied by DTA, TGA and DTG and is shown in Fig. 2(b). Thermal analysis of the activated carbon material gives a view about the change of mass, enthalpy and thermal capacity. TGA measure the weight gain or loss as a function of temperature. Information regarding sample composition and its thermal stability can be derived from the TGA data. DTG shows the most evident weight loss temperature of the SbAC. DTA data shows phase transition of the material. 10.48 mg of synthesized SbAC material is heated from 24 °C till 700 °C at a heating rate of 10 °C /min in inert atmosphere (N_2 gas at a rate of 200 ml/min). The gradual mass loss occurs in two steps when heated at constant rate as shown in TGA curve. The first mass loss (up to 25%) of SbAC occurs at low temperature to ($20 < T < 100$ °C). This is due to extractive compounds evaporation, desorption of physically adsorbed water on the material and moisture loss. After this very less weight loss occurs till 450 °C. Next big weight loss step occurs at 500 °C. This mass loss at such high temperature can be assigned to the decomposition of various functional groups present in the SbAC such as ethers, phenols, esters and quinones etc. The presence of these functional groups is also confirmed from the FTIR study (Fig. 2(d)). The presence of two knee points in the TGA graph is also confirmed by the corresponding DTG graph. The DTA curve shown along with TGA and DTG shows an endothermic peak at low temperature due to desorption of moisture from the sample as evident from the TGA plot.

The specific structure nature of the SbAC was investigated by the Raman spectroscopy shown in Fig. 2(c). Low laser power (50 mW) was used for taking the measurements at a spectral resolution of 3 cm^{-1}. The signal was detected by a CCD system. Fig. 2(c) shows two intense bands positioned at 1334 cm^{-1} and at 1580 cm^{-1} ascribed to vibrational modes. These vibrational modes involve the sp^2 bonded carbon atoms of the disordered microcrystalline domain. The peak at around 1334 cm^{-1} (D-band, D-defects and disorder) is attributed to the breathing mode of k-point phonons (A_{1g} symmetry). This corresponds to the defective graphitic structures or disordered form of carbon

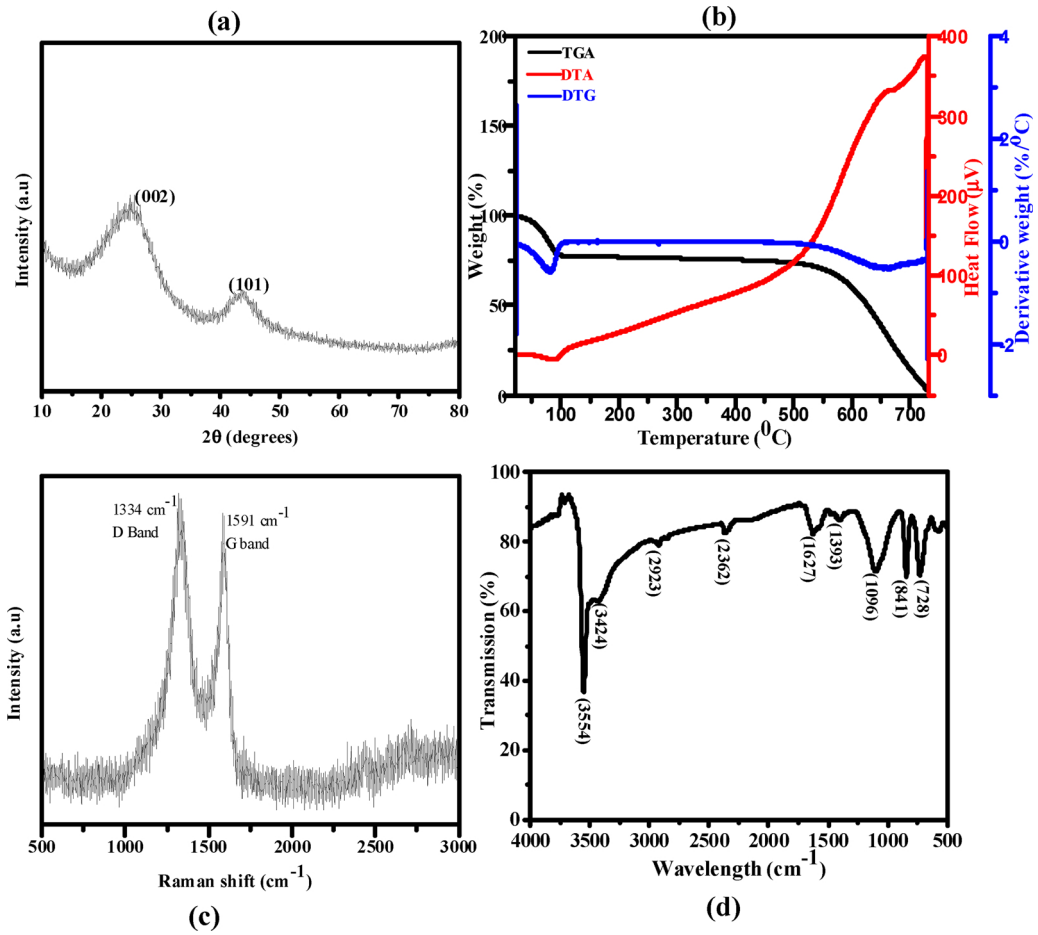

Fig. 2. (a) XRD pattern, (b) TGA, DTA and DTG (c) Raman spectra and (d) FTIR spectra of S. bengalense derived activated carbon (SbAC).

materials. Raman spectroscopy is considered as a sensitive technique for finding disorders in sp^2 carbon materials because disorder in sp^2 hybridized carbon systems gives rise to resonance in Raman spectra. The band centered at 1591 cm^{-1} (G-band, G-graphite) is attributed to the E_2g mode of the Γ-point. The stretching of the C−C bond in graphitic materials forms G-band and this is common for all sp^2 carbon systems. The intensity ratios of the two peaks I_D/I_G partially depend on the graphitization degrees, and the higher value of the I_D/I_G indicates higher electrical conductivity. Fig. 2(c) shows that the ratio of I_D/I_G is approximately one indicating the amorphous nature of SbAC.

FTIR measurements of the AC are considered very important because they provide information about various functional groups present in the material. Moreover, the adsorption property of the AC is greatly influenced by these functional groups. The FTIR spectra of SbAC was difficult to obtain due to problems in the sample preparation and poor transmittance hence the spectra of carbon materials generally show unavoidable distortions which makes the data interpretation complicated [23]. Fig. 2(d) shows the FTIR spectra of the prepared activated carbon sample in the wavenumber range of 500–4000 cm^{-1} which indicates the presence of oxygen containing functional groups such as carbonyl groups, hydroxyl groups and carboxyl groups. Table 1 shows the functional groups and their corresponding wavenumbers present in SbAC.

A strong and broad peak at 3554 cm^{-1} and a weak peak at 3424 cm^{-1} are found in the obtained spectra. These two peaks may be assigned to the O−H stretching. This O−H stretching may be due to the presence of polymeric compounds in the SbAC such as phenols, alcohols and carboxylic acids. The intermolecular hydrogen bonding due to the O−H stretching shows that the free hydroxy groups are present on the carbon surface [24,25]. There were two more weak peaks at 2923 cm^{-1} and at 2362 cm^{-1} corresponding to C−H stretching in CH_2 groups and to C−O bonds in ketene groups respectively [26]. The peak observed around 1627 cm^{-1} may be due to C=C stretching vibrations in aromatic rings improved by polar functional groups [26]. The intensity of this band would be strengthened by the oxygen atoms presence, probably due to an increase in the dipole moment of the ring vibrations [27]. The strong and broad peak in the 1300–1000 cm^{-1} region is due to the overlapping of many bands in vibrational modes. This peak may be due to the presence of alkyl groups and the bending vibrations of its C−H group. They can be CH_3 of lignin and collective modes of the carbonaceous C−C skeleton and the stretching vibration of phosphonate groups [28,29]. The strong peak at 1096 cm^{-1} may be due to CO single bonds for instance those in phenols, ethers, esters and acids [26]. Two more strong peaks at 841 cm^{-1} and 728 cm^{-1} were found which can be related to the IR spectra some condensed rings such as of C−H [30].

Table 1
Functional groups present in SbAC.

Wavenumber (cm^{-1})	Functional groups
3554	Alcohol O−H stretching
3424	Carboxylic acid O−H stretching, Alcohol O−H stretching
2923	sp^3 C-H Asymmetric stretching
2362	carbon-oxygen bonds in ketene groups
1627	C=C Aromatic skeletal stretching, C=C Alkene stretching, C=O stretching
1393	sp^3 C−H bend
1096	C−O alkoxy
841&728	Alkene sp^2 C−H bend, aromatic sp^2 stretch

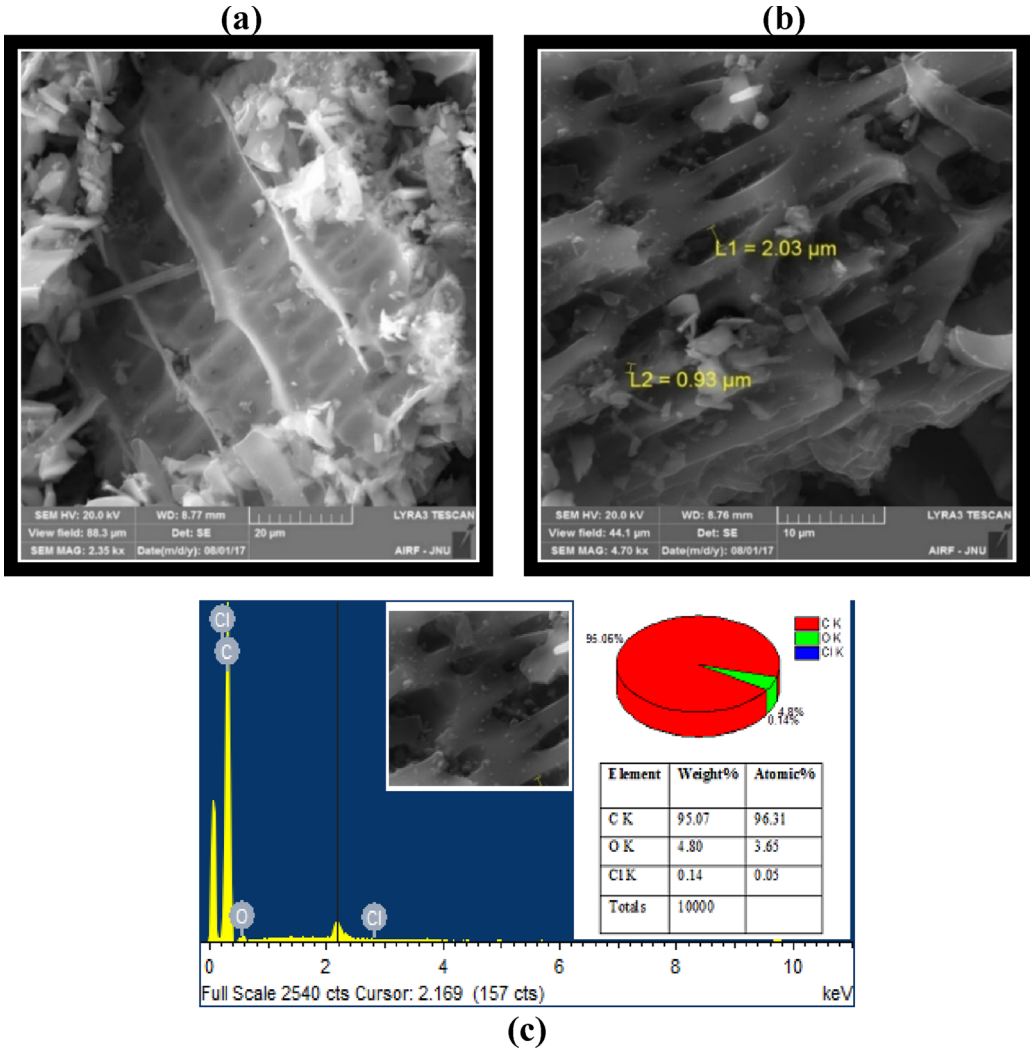

Fig. 3. (a) FESEM images of S. bengalense derived activated carbon (SbAC) at different magnification (b) FESEM-EDX spectrum of SbAC.

The surface morphology of the as prepared SbAC is shown in Fig. 3(a) and (b) at different magnifications (20 µm and 10 µm respectively).

It is observed that the synthesized SbAC is porous in nature. Furthermore, this kind of good porous structure allows the electrolyte (1 M Li_2SO_4) ions to diffuse easily through the carbon materials by decreasing the resistance to the interior for electrolyte ions and get adsorbed there on the surface. Hence, these homogeneously distributed pores of grains and pores surface in the synthesized SbAC material are responsible for high specific surface area. The specific surface area value and pore diameters are further determined by N_2 adsorption-desorption and discussed in the next sections. EDX elemental distribution of SbAC shown in Fig. 3(c), clearly shows the ignorable presence of elements other than carbon.

For the activation process of SbAC $ZnCl_2$ is chosen. During activation process dissolution of $ZnCl_2$ in water leads to decrease in pH due to protons released from the solvation of zinc ions and $ZnCl_2$ causes degradation of cellulose and lignin of the lignocellulosic material.

$$Zn[H_2O]_6^{+2} \leftrightharpoons ZnOH[H_2O]_5^{+} + H^{+}$$

During the initial stage of $ZnCl_2$ large amount of water is released due to dehydration reactions of $ZnCl_2$. The oxygen containing functional groups such as OH groups reacts with $ZnCl_2$ to form Zn-O complexes [31]. Further heating causes vaporisation of oxygen and hydrogen from the precursor and decomposition of $ZnCl_2$ into Zn and Cl_2. Heating at a temperature greater than the melting point of $ZnCl_2$ i.e. 732 °C carbon atoms interact with the Zn species and this interaction causes the widening the carbon layers which results in the creation of pores and the formation of porous structure.

The detailed quantitative analysis of the effects of chemical activation on specific surface area of SbAC and other porosity parameters are calculated using N_2 adsorption-desorption characterization. The N_2 adsorption-desorption isotherm of the synthesized SbAC is shown in Fig. 4 and the pore size distribution is shown in the inset. The synthesized carbon material shows the type-I isotherm according to the IUPAC classification. After the abrupt rise at very low-pressure values ($P/P_0 \sim 0.003$), there is a steady increase in adsorption then for the whole range of P/P_0. The steep rise at the beginning of the isotherm is due to the major uptake of nitrogen gas and indicates that SbAC has a considerable large portion of micropores and indicated good microporosity whereas the steady increase after the initial jump is the indication of the existence of mesopores. The pore size distribution of the SbAC was calculated by using the Barrett-Joyner-Halenda (BJH) method [32] with desorption data which is shown in the inset of Fig. 4. Quantitative approximations of the micro and mesopore volumes,

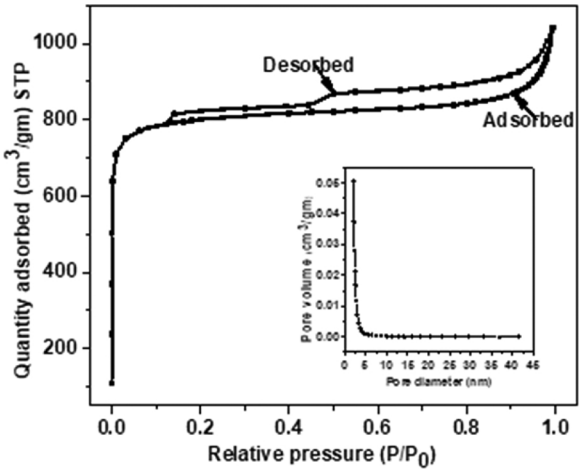

Fig. 4. N_2 adsorption-desorption isotherm and the pore size distribution (inset) of SbAC.

specific surface area and average pore size are listed in Table 2.

From the plot and table, it is observed that the pores in the SbAC falls in the category of mesopores because the average pore size calculated is 2.05 nm and micropore area is greater than the mesopore area.

The surface area and porosity parameters are largely dependent on activating agents used for the activation process. Different kinds of activating agents have been explored for the chemical activation method which are broadly divided into three classes i.e. a strong base (KOH, NaOH) an acid [HNO_3, H_3PO_4,$(NH_4)_2SO_8$] or a salt (H_2O_2, $KMnO_4$, $ZnCl_2$, KCl, K_2CO_3) and steam in the literature. Out of the above-mentioned activating KOH, H_3PO_4 and $ZnCl_2$ are the most studied whereas KOH is generally used for the synthesis of activated carbon from chars and coals and it gives microporous kind of structure. H_3PO_4 and $ZnCl_2$ are preferred for the biomass resources or lignocellulosic materials as they form both microporous and mesoporous structures. H_3PO_4 is preferred if the final activated carbon obtained has to be used for pharmaceutical and food industries applications. $ZnCl_2$ shows high reactivity with the lignocellulosic material due to the presence of −OH groups in the lignocellulosic materials. The activated carbon synthesized in this work will be used for supercapacitor applications hence $ZnCl_2$ is preferred over phosphoric acid as $ZnCl_2$ gives higher specific area as compared to phosphoric acid [33]. These days more and more research groups are preferring $ZnCl_2$ over other activating agent for the synthesis of activating carbon from biomass resources due to its substantial effect on the pore structure, pore size and surface area by varying the concentration of $ZnCl_2$ [34]. R. Chen *et al* used K_2CO_3, KOH and $ZnCl_2$ activating agent for the synthesis of activated carbon from tobacco stem and found that out of the three $ZnCl_2$ gave better porosity with specific surface area up to 1347 $m^2 g^{-1}$ [35]. J. Zhang *et al* synthesized activated carbon by $ZnCl_2$ activating agent from Camellia oleifera shell of high porosity with specific surface area upto 1935 $m^2 g^{-1}$ [36].

Therefore, it can be concluded that the presence of mesoporous along with microporous structure in SbAC makes it good material for EDLC electrodes.

3.2. Electrochemical performances

This section presents the electrochemical properties of the as synthesized SbAC. The supercapacitor cells were made by 2 electrode geometry configurations and were tested for their performance in aqueous electrolyte 1 M Li_2SO_4 and the results are discussed in next section.

The electrochemical behaviour of the SbAC based EDLC cells were tested by the cyclic voltammetry (CV) measurements over the increasing potential ranges from 0.8 V to 1.6 V. The recorded CV responses for the different potential ranges are depicted in Fig. 5(a). It may be noted that with increasing potential ranges from 0.8 V to 1.6 V, the cyclic voltammetry curves show quasi-rectangular kind of shape. This kind of shape (quasi-rectangular) of cyclic voltammetry favours the formation of double layer for the electric double layer capacitors applications. But for 1.6 V and above the CV curves starts deviating from this quasi-rectangular shape. This can be due to the decomposition voltage of 1 M Li_2SO_4 as it shows the decomposition voltage of 1.8 V. Hence, the operating voltage range for the devices made from SbAC can be up to 1.6 V and if operated beyond this value of potential the device performance will get deteriorated due to the decomposition of the electrolyte.

The SbAC electrodes have also been tested to study their constant current charge-discharge properties. Fig. 5(b) shows the charge discharge behaviour of the electrodes at different voltages (0.8, 1.0, 1.2, 1.4, and 1.6 V) for a constant current value of 200 mA/g. All the discharge plots in Fig. 5(b) shows a linear and symmetrical variation. This behaviour confirms the good capacitive behaviour of the EDLC cells.

The electrochemical stability window (ESW) defines the electrochemical working voltage range of the electrolyte. The ESW of Li_2SO_4 is found to be ~ 1.0 V and the safest voltage limit of electrical double layer is 0.8 V in aqueous electrolytes with activated carbons. Beyond that the electrode-electrolyte reactions come in to the picture. The electrolytes play an important role in charge storage and determining the energy and power density of EDLC. Aqueous, ionic liquids and organic electrolytes can be used for the EDLCs. Each electrolytes system has its merits and demerits. Out of the three types of electrolytes organic and ionic liquids have large electrochemical window or decomposition voltage (the maximum voltage an electrolyte can sustain) but they have then high viscosity and are costlier too. Due to the high viscosity ionic liquids have higher value of the equivalent series resistance which becomes a hindrance for their applications in EDLCs. Though aqueous electrolytes have small electrochemical window as compared to organic and ionic liquids but they are very cheap, environment friendly, non-corrosive and have low viscosity and good ionic conductivity. Therefore, aqueous electrolytes are the most studied electrolytes for EDLCs. Both the electrolytes i.e. alkali (e.g. NaOH, KOH) and acids (e.g. Li_2SO_4, Na_2SO_4, K_2SO_4 and H_2SO_4) have been used for EDLCs. Li_2SO_4 is the most studied aqueous electrolyte and shows decomposition voltage of 1.8 V due to stronger hydration of Li^+ compared to Na^+ and K^+ ions. If the operating voltage is increased above this, CV curve starts showing decomposition peak.

Fig. 5(c) shows the Nyquist plots or electrochemical impedance spectroscopy (EIS) of SbAC electrodes in 1 M Li_2SO_4 aqueous electrolyte to understand the charge transfer resistance. The plot shows that the imaginary values img Z or Z″ increases abruptly with respect to its real part real Z (Z′) for the frequency variation from high (100 kHz) to low

Table 2
: Porosity parameters and specific surface area of the SbAC evaluated from N_2 adsorption–desorption isotherm.

BET specific area ($m^2 g^{-1}$)	mesopore area ($m^2 g^{-1}$)	micropore area ($m^2 g^{-1}$)	mesopore volume ($cm^3 g^{-1}$)	micropore volume ($cm^3 g^{-1}$)	average pore size (nm)
2090	290	1800	0.049	0.281	2.05

values (10 mHz) as shown in the inset of the Fig. 5(c). The figure exhibits a small semicircle diameter line followed by an inclined line for low frequency region. This specifies the capacitive behaviour of the SbAC based EDLC cells under the present studies. This corresponds to the creation of a compatible interface between SbAC electrode/electrolyte thereby providing easy access for the electrolyte ions towards the electrode. Many electrical parameters which are related to the bulk parameters or properties of the electrode-electrolyte interfaces and electrolyte scan be calculated by using impedance measurements for different values of frequencies.

The specific capacitance values of the material were calculated by the following equations.

$$C_s = \frac{i}{ms} \tag{1}$$

where i is the average current, m is the mass of the material and s is the scan rate of the applied ramp voltage (Vs^{-1}). Eq. (1) can be written as

$$C_s = \frac{i\Delta t}{m\,\Delta V} \tag{2}$$

In the above eqn. i is the applied current (A) and Δt is taken as the time interval of the voltage change (ΔV) for the capacitor cells and m here is the actual mass of the material.

The specific capacitance of SbAC electrodes are calculated from galvanostatic charge-discharge curves using a constant current density using Eq. (2). The specific capacitance values plotted against increasing potential range (0.8, 1.0, 1.2, 1.4, and 1.6 V) for a constant current value of 200 mA/g and are shown in Fig. 5(d). It is observed that the specific capacitance values increase from 96 F g^{-1} for 0.8 V to 102.6 F g^{-1} for maximum voltage of 1.6 V. So, the specific capacitance values of the cell increases along with the operating potential range values (0.8, 1.0, 1.2, 1.4, and 1.6 V) and the highest specific capacitance value 102.6 F g^{-1} is obtained for 1.6 V operating potential. The value of the areal and volumetric capacitance is also calculated and is found to be 30.8 m F cm^{-2} and 1540 m F cm^{-3} respectively. It can be concluded from Fig. 5(d) that the specific capacitance of SbAC cell increases for large cell voltage range. Various kinds of biomass resources have been studied for the production of activated carbon using $ZnCl_2$ as the activating agent for supercapacitor applications. J. Zhang *et al* used waste camellia oleifera shell as a precursor for the production of activated carbon with $ZnCl_2$ activation to be used for EDLCs applications. The electrochemical study performed in aqueous electrolyte showed specific capacitance up to 374 F g^{-1} in H_2SO_4 [37]. Cow dung has also been used for the synthesis of activated carbon and the synthesized activated carbon showed good specific capacitance (124 F g^{-1}) at low current density (0.1 A g^{-1}) [38]. Activated carbon obtained from sugar cane bagasse (a waste from the sugar cane or Saccharum officinarum plant) by chemical activation using $ZnCl_2$ exhibits good specific aenergy density and high specific capacitance 300 F g^{-1} [39].

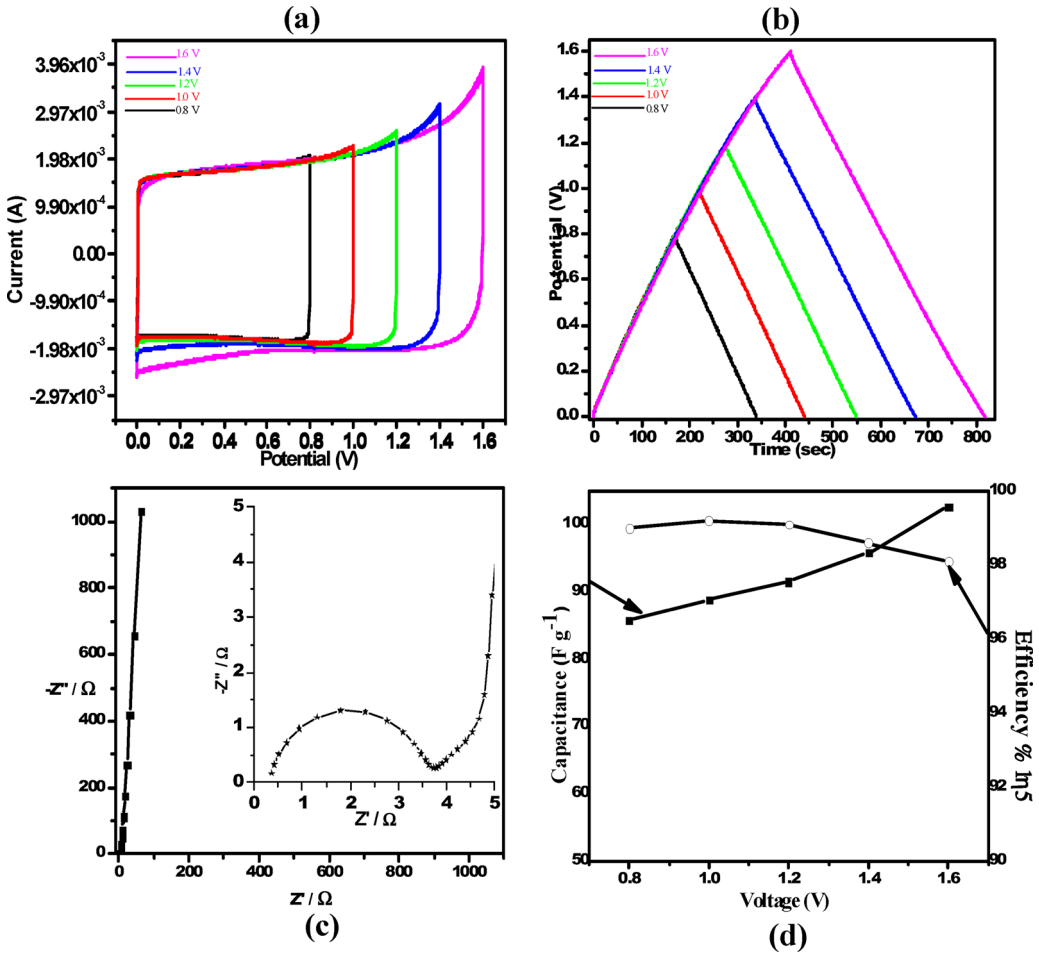

Fig. 5. (a) Cyclic voltammogram of supercapacitor cell with increasing voltage range at constant scan rate 2 mV/s at room temperature. (b) Galvano static charge-discharge curves of activated carbon powder electrodes at constant current of 200 mA/g. (c) Nyquist plot of SbAC recorded at room temperature. The expanded impedance plot is shown as insets. (d) Variation of the specific capacitance and efficiency of supercapacitive cell as a function of cell voltage.

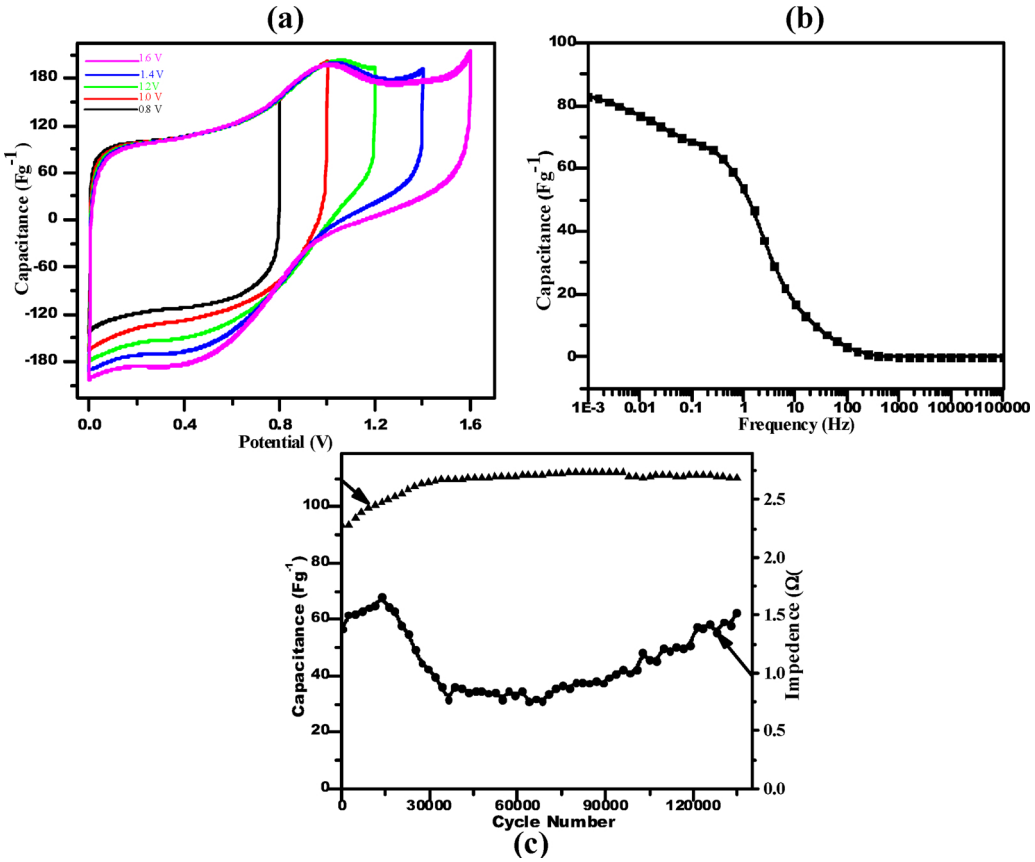

Fig. 6. (a) Cyclic voltammogram of supercapacitor cell after 120,000 cycles. (b) Frequency dependence of the specific capacitance of SbAC. (c) Comparative graphs showing the variation of specific capacitance and impedance of supercapacitive cell with cycle numbers.

To calculate the Coulombic efficiency η the following equation is used.

$$\eta = \frac{t_D}{t_C} \times 100\,\% \tag{3}$$

In Eq. (3), t_D and t_C represents the times of galvanostatic discharging and galvanostatic charging, respectively [40]. The efficiency calculated using Eq. (3) is plotted against increasing potential (shown in Fig. 5(d)). The efficiency value approximately 99% for low voltage values (0.8 V, 1.0 V and 1.2 V) but decreases to approximately to 98% at higher voltages (1.6 V). Hence, there is only slight variation in efficiency for different potential range.

The capacitor cells fabricated with SbAC are characterized for very large number of charge-discharge cycles (up to 120,000 cycles). Fig.6 (a) shows the variation of cyclic voltammogram of supercapacitor cell after 120,000 cycles for increasing voltage range at constant scan rate 2 mV/s at room temperature. If the CV response of SbAC based cells after 120,000 cycles (Fig. 6(a)) is compared with CV response recorded for the same material for the 1 st cycle (Fig. 6(a)) then it can be concluded that after 120,000 cycles the shape of the CV response gets completely distorted from the quasi rectangular shape.

In addition to quasi rectangular shape some redox peaks can also be seen in Fig. 6(a) which is generally ascribed to pseudo-Faradic reactions occurring due to the presence of some oxygenated groups (such as quinone, carboxyl and phenolic group) in the electrode material. The presence of these oxygenated groups can be confirmed from the FTIR results in the manuscript (Fig. 2(d) and Table 1). Another reason the becoming this hump more prominent at higher potential can be related to the electro-oxidation of trapped hydrogen in the pores of the electrode material i.e. activated carbon. After being operated for many cycles the electrolyte ions may not be able to get completely desorbed from the pores and which may decrease the performance of the cell.

Fig. 6(b) displays the variation of the specific capacitance of the SbAC based cells with frequency. It is observed that the capacitance attains its maximum at the low frequency as at such low frequency the electrolyte ions can get the sufficient time to move to the pores to get adsorbed there and then form the double layer on the electrode surface.The capacitance value at the lowest frequency henceforth represents the total capacitance of the double layer interface (C_{dl}). The specific capacitance 82 F g^{-1}decreases to around 3 F g^{-1} at 100 Hz and becomes very low if the frequency is increased further. At high frequencies C_{dl} contributes less because at such high frequencies more ions are not able to transport, and hence at such high frequency the main contribution is due to the bulk electrolyte's process (C_{bulk}).

As discussed earlier along with high value of capacitance, energy density and power density and good cycle life are also main features of the EDLCs. An EDLC that exhibits high cycle life is considered a good capacitor because it increases the life of the power device. The variation of the specific capacitance of the SbAC based electrodes as a function of charge-discharge cycles up to 120,000 cycles is shown in Fig. 6(c). It can be concluded from the figure that after initial decrease for limited cycles, the specific capacitance increases to maximum value and then starts decreasing. There can be loosely bound ions such as OH^- on the electrode surface and when the charges are consumed in these loosely bound ions in irreversible reactions, they give rise to decrease in the specific capacitance after few cycles. Another reason for this initial drop in specific capacitance after few cycles can be the permanent filling of some micropores on the SbAC electrode surface. Irreversible redox reaction of some functional groups present at the electrode surface can also be responsible for the same.

The variation in the impedance (includes over-all resistance, internal resistance, and ESR etc) of the cell for different charge-discharge

cycles is tested and is shown in Fig. 6(c). It can be observed from the graph that after initially there is small increase in ESR and then it becomes stable after that. The bulk resistance of the electrolyte does not change with cycling much. The ions transport is facile through the electrolyte and the interface. The electrode material does not introduce the additional pore resistance on cycling. This constant impedance ensures the constant power delivery throughout the cycling. Initial ohmic drop for ESR value of the SbAC cell during constant current discharge may cause the voltage drop.

4. Conclusion

In summary, the synthesized highly porous activated carbon using Saccharum bengalense (S. bengalense) leaves (SbAC) by $ZnCl_2$ activation. The synthesized SbAC shows good specific surface area of value 2090 $m^2 g^{-1}$, total mesopore volume of 0.049 $cm^3 g^{-1}$, total micropore volume of 0.281 $cm^3 g^{-1}$of and the larger percentage of micropores of average size 2.05 nm provides more reaction sites at the electrode surface for the electrolyte ions. The high value of surface area is favourable for the performance of the EDLC and specific capacitance value of 102.6 F $g^{-1}$is obtained at a scan rate of 2 mV/s in aqueous electrolyte (1 M Li_2SO_4) for 1.6 V operating voltage. SbAC shows good cycling stability up to 120,000 cycles. The chemical activation method used here for the synthesis of SbAC with $ZnCl_2$ activating agent is very simple and cheap. All these results establish that the *Saccharum bengalense (S. bengalense)* leaves derived activated carbon (SbAC) activated carbon can be a good candidate for EDLC electrode material for energy storage technology.

Acknowledgements

The authors acknowledge the financial support obtained from the Science and Engineering Research Board (SERB), Department of Science and Technology (DST), Govt. of India (sanction no. ECR/2016/001871) under the scheme Early Career Research Award.

Appendix A. Supplementary data

Supplementary material related to this article can be found, in the online version, at doi:https://doi.org/10.1016/j.est.2018.10.009.

References

[1] P. Kossyrev, Carbon black supercapacitors employing thin electrodes, J. Power Sources 201 (2012) 347–352.
[2] M. Minakshi, D. Meyrick, D. Appadoo, Maricite ($NaMn_{1/3}Ni_{1/3}Co_{1/3}PO_4$)/Activated carbon: hybrid capacitor, Energy Fuels 27 (2013) 3516–3522.
[3] M. Minakshi, M.J. Barmia, R.T. Jones, Rescaling metal molybdate nanostructures with biopolymer for energy storage having high capacitance with robust cycle stability, Dalton Trans. 46 (2017) 3588–3600.
[4] R. Ramkumar, M.M. Sundaram, Electrochemical synthesis of polyaniline cross linked $NiMoO_4$ Nanofibre Dendrites for energy storage devices, New J. Chem. 40 (2016) 7456–7464.
[5] K. Shi, M. Ren, I. Zhitomirsky, Activated carbon-coated carbon nanotubes for energy storage in supercapacitors and capacitive water purification, ACS Sustain. Chem. Eng. 2 (2014) 1289–1298.
[6] K. Shi, I. Zhitomirsky, Asymmetric supercapacitors based on activated-carbon coated carbon nanotubes, ChemElectroChem 2 (2015) 396–403.
[7] K. Shi, I. Zhitomirsky, Influence of chemical structure of dyes on capacitive dye removal from solutions, Electrochim. Acta 174 (2015) 588–595.
[8] L. Wei, G. Yushin, Nanostructured activated carbons from natural precursors for electrical double layer capacitors, Nano Energy 1 (2012) 552–565.
[9] W. Lu, R. Hartman, L. Qu, L. Dai, Nanocomposite electrodes for High performance supercapacitors, J. Phys. Chem. Lett. 2 (2011) 655–660.
[10] E. Frackowiak, Supercapacitors based on carbon materials and Liquids, J. Braz. Chem. Soc. 17 (2006) 1074–1082.
[11] A.B. Fuertes, M. Sevilla, Hierarchical microporous/mesoporous carbon nanosheets for High-performance supercapacitors, ACS Appl. Mater. Interfaces 7 (2015) 4344–4353.
[12] T.E. Rufford, D.H. Jurcakova, Z. Zhu, G.Q. Lu, Nanoporous carbon electrode from waste coffee beans for high performance supercapacitors, Electro. Chem. Commun. 10 (2008) 1594–1597.
[13] A.E. Ismanto, S. Wang, F.E. Soetaredjo, S. Ismadji, Preparation of capacitor's electrode from cassava peel waste, Bioresour. Technol. 101 (2010) 3534–3540.
[14] J. Hayashi, T. Horikawa, I. Takeda, K. Muroyama, F.N. Ani, Preparing activated carbon from various nutshells by chemical activation with K_2CO_3, Carbon 40 (2002) 2381–2386.
[15] K.Y. Foo, B.H. Hameed, Utilization of rice husks as a feedstock for preparation of activated carbon by microwave induced KOH and K_2CO_3 activation, Bioresour. Technol. 102 (2011) 9814–9817.
[16] X. Li, W. Xing, S. Zhuo, J. Zhou, F. Li, S.Z. Qiao, Preparation of capacitor's electrode from sunflower seed shell, Bioresour. Technol. 102 (2011) 1118–1123.
[17] J.M.V. Nabais, J.G. Teixeira, I. Almeida, Development of easy made low cost bindless monolithic electrodes from biomass with controlled properties to be used as electrochemical capacitors, Bioresour. Technol. 102 (2011) 2781–2787.
[18] E. Taer, M. Deraman, I.A. Talib, A. Awitdrus, S.A. Hashmi, A.A. Umar, Preparation of a highly porous binderless activated carbon monolith from rubber wood sawdust by a multi-step activation process for application in supercapacitor, Int. J. Electrochem. Sci. 6 (2011) 3301–3315.
[19] W. Tian, Q. Gao, Y. Tan, et al., Bio-inspired beehive-like hierarchical nanoporous carbon derived from bamboo based industrial by-product as a high-performance supercapacitor electrode material, J. Mater. Chem. A 3 (2015) 5656–5664.
[20] X. He, P. Ling, J. Qiu, M. Yu, Zhang X, C. Yu, M. Zheng, Efficient preparation of biomass-based mesoporous carbons for supercapacitors with both high energy density and high-power density, J. Power Sources 240 (2013) 109–113.
[21] Z. Hu, M.P. Srinivasan, Y. Ni, Preparation of mesoporous high-surface-area activated carbon, Adv. Mater. 12 (2000) 62–65.
[22] J.H. Hou, C.B. Cao, F. Idrees, X.L. Ma, Hierarchical porous nitrogen-doped carbon nanosheets derived from silk for ultrahigh-capacity battery anodes and supercapacitors, ACS Nano 9 (2015) 2556–2564.
[23] A. Lazzarini, A. Piovano, R. Pellegrini, G. Leofanti, G. Agostini, S. Rudic, M.R. Chierotti, R. Gobetto, A. Battiato, G. Spoto, A. Zecchina, C. Lambertiah, E. Groppo, A comprehensive approach to investigate the structural and surface properties of activated carbons and related Pd-based catalyst, Catal. Sci. Technol. 6 (2016) 4910–4922.
[24] J.F. Gonzalez, S. Roman, C.M.G. Garcia, J.M.V. Nabais, J.M. Valente, A.L. Ortiz, Porosity development in activated carbons prepared from walnut shells by carbon dioxide or steam activation, Ind. Eng. Chem. Res. 48 (2009) 7474–7481.
[25] P.E. Fanning, M.A. Vannice, A drifts study of the formation of surface groups on carbon by oxidation, Carbon 31 (1993) 721–730.
[26] Puziy A.M, O.I. Poddubnaya, A.M. Alonso, F.S. Garcia, J.M.D. Tascon, Synthetic carbons activated with phosphoric acid I. Surface chemistry and ion binding properties, Carbon 40 (2002) 1493–1505.
[27] A.G.D. Prasad, J.K. Kumar, P. Sharanappa, Fourier transform infrared spectroscopic study of rare and endangered medicinal plants Romanian, J. Biophys. 21 (2011) 221–230.
[28] A.P. Terzyk, The influence of activated carbon surface chemical composition on the adsorption of acetaminophen (paracetamol) in vitro part II. TG, FTIR, and XPS analysis of carbons and the temperature dependence of adsorption kinetics at the neutralpH, Colloids Surf. A: PhysicochemEng Aspects 177 (2001) 23–45.
[29] Z.A. Qodah, R. Shawabkah, Production and characterization of granular activated carbon from activated sludge, Braz. J. Chem. Eng. 26 (2009) 127–136.
[30] A.C. Ferrari, S.E. Rodil, J. Robertson, Interpretation of infrared and Raman spectra of amorphous carbon nitrides, Phys. Rev. B 67 (2003) 155306–155326.
[31] T.E. Rufford, D.H. Jurcakova, J. Zhu, Green Carbon Materials Advances and Applications, Pan Stanford Publishing, 2013, p. 45.
[32] H. Marsh, F.R. Reinoso, Activated Carbon, 1st edn, Elsevier Science Tech Books, 2006.
[33] J.M. Thomas, W.J. Thomas, Principles and Practice of Heterogeneous Catalysis, VCH VerlagsgesellschaftmbH, Weinheim, Federal Republic of Germany, 1997, pp. 267–275.
[34] Y. Onal, C.A. Basar, C.S. Ozdemir, J. Hazard. Mater. 148 (2007) 727–734.
[35] R. Chen, L. Li, Z. Liu, M. Lu, C. Wang, H. Li, W. Ma, S. Wang, J. Air Waste Manag. Assoc. 67 (2017) 713–724.
[36] J. Zhang, L. Gong, K. Sun, J. Jiang, X. Zhang, J. Solid State Electrochem. 16 (2012) 2179–2186.
[37] J. Zhang, L. Gong, K. Sun, J. Jiang, X. Zhang, Preparation of activated carbon from waste Camellia oleifera shell for supercapacitor application, J. Solid State Electrochem. 16 (2012) 2179–2186.
[38] D. Bhattacharjya, J.S. Yu, Activated carbon made from cow dung as electrode material for electrochemical double layer capacitor, J. Power Sources 262 (2014) 224–231.
[39] T.E. Rufford, D.H. Jurcakova, K. Khosla, Z. Zhu, G.Q. Lu, Microstructure and electrochemical double-layer capacitance of carbon electrodes prepared by zinc chloride activation of sugar cane bagasse, J. Power Sources 195 (2010) 912–918.
[40] M. Suleman, Y. Kumar, S.A. Hashmi, Flexible electric double-layer capacitors fabricated with micro-/mesoporous carbon electrodes and plastic crystal incorporated gel polymer electrolytes containing room temperature ionic liquids, J. Solid State Electrochem. 19 (2015) 1347.